Bulletin of the Seismological Society of America, Vol. 94, No. 6, pp. 2299–2316, December 2004

Evidence for Late Holocene Earthquakes on the Utsalady Point Fault, Northern Puget Lowland, Washington

by Samuel Y. Johnson, Alan R. Nelson, Stephen F. Personius, Ray E. Wells, Harvey M. Kelsey, Brian L. Sherrod, Koji Okumura, Rich Koehler III, Robert C. Witter, Lee-Ann Bradley, and David J. Harding

Abstract Trenches across the Utsalady Point fault in the northern Puget Lowland of Washington reveal evidence of at least one and probably two late Holocene earthquakes. The "Teeka" and "Duffers" trenches were located along a 1.4-km-long, 1- to 4-m-high, northwest-trending, southwest-facing, topographic scarp recognized from Airborne Laser Swath Mapping. Glaciomarine drift exposed in the trenches reveals evidence of about 95 to 150 cm of vertical and 200 to 220 cm of left-lateral slip in the Teeka trench. Radiocarbon ages from a buried soil A horizon and overlying slope colluvium along with the historical record of earthquakes suggest that this faulting occurred 100 to 400 calendar years B.P. (A.D. 1550 to 1850). In the Duffers trench, 370 to 450 cm of vertical separation is accommodated by faulting (~210 cm) and folding (~160 to 240 cm), with probable but undetermined amounts of lateral slip. Stratigraphic relations and radiocarbon ages from buried soil, colluvium, and fissure fill in the hanging wall suggest the deformation at Duffers is most likely from two earthquakes that occurred between 100 to 500 and 1100 to 2200 calendar years B.P., but deformation during a single earthquake is also possible. For the two-earthquake hypothesis, deformation at Teeka trench in the first event involved folding but not faulting. Regional relations suggest that the earthquake(s) were $M \geq \sim 6.7$ and that offshore rupture may have produced tsunamis. Based on this investigation and related recent studies, the maximum recurrence interval for large ground-rupturing crustal-fault earthquakes in the Puget Lowland is about 400 to 600 years or less.

Introduction

Forearc regions of convergent continental margins are subject to earthquakes from sources on the subduction zone interface, in the downgoing slab, and on shallow faults in the upper plate. Recent large, damaging earthquakes such as the 1995 *M* 6.9, Kobe, Japan earthquake (e.g., Kanamori, 1995; Pollitz and Sacks, 1997), illustrate the significant seismic hazard presented by shallow forearc faults and the importance of understanding the histories of these faults for accurate hazard assessment.

Documenting the earthquake histories of shallow faults in the densely populated Puget Lowland forearc region of the Cascadia convergent margin is in its early stages. Recognition and documentation of active tectonic landforms, which is necessary for paleoseismologic investigations, is difficult because of dense forest cover and the relatively young (<16 ka), postglacial age of the landscape. Several postglacial fault scarps have recently been identified in the Puget Lowland using Airborne Laser Swath Mapping (ALSM) surveys (i.e., LIDAR), which can image low-relief landforms beneath forest canopies (Harding and Berghoff, 2000; Haugerud *et al.*, 2003). Trenching investigations of ALSM-imaged backthrusts to the Seattle fault have documented three to four large, ground-rupturing earthquakes in the past ~2500 years (Nelson *et al.*, 2002, 2003). This report describes a trench investigation of an ALSM-recognized scarp along the Utsalady Point fault (Johnson *et al.*, 2001, 2003) in the northern Puget Lowland. Trench data indicate vertical and left-lateral fault offsets in a large earthquake that occurred about 400 to 100 calendar years (cal yr) B.P., and probably a second earthquake that occurred between about 2200 and 1100 cal yr B.P.

Regional Tectonics and the Utsalady Point Fault

Northwestern Washington (Fig. 1) lies within the structurally complex continental margin of the Pacific Northwest (e.g., Johnson *et al.*, 2003). Oblique northeast-directed convergence of the Juan de Fuca plate below the North America plate, along with larger-scale shearing of the Pacific plate against North America, are driving forces for crustal faulting

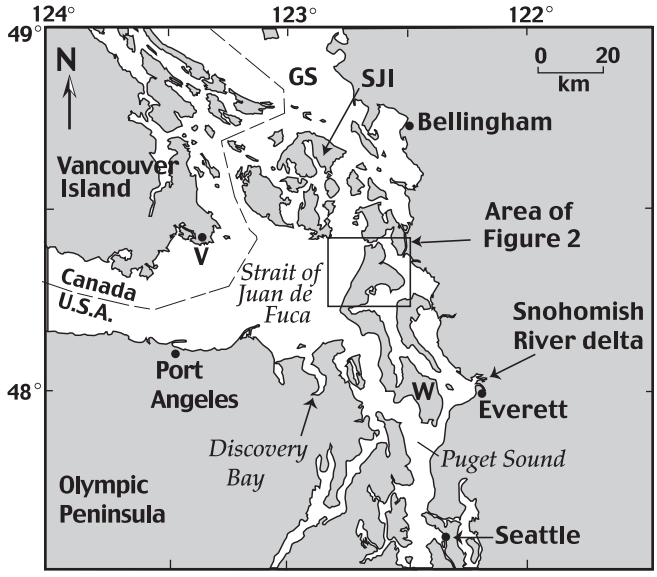

Figure 1. Map showing parts of northwestern Washington and southwestern British Columbia, including area of Figure 2. GS, Georgia Strait; SJI, San Juan Islands; W, Whidbey Island; V, Victoria.

and deformation in the region (Wells *et al.*, 1998). The Washington Coast Range, floored by Eocene marine basaltic rocks, is part of a forearc sliver that is moving northward relative to pre-Tertiary basement rock in the Cascade Range to the east. In Washington, the boundary between these two terranes cuts through the Puget Lowland, an elongate forearc basin. In the northern Puget Lowland, the northwest-trending southern Whidbey Island fault represents part of this contact (Johnson *et al.*, 1996). Farther west on Vancouver Island, the forearc sliver is buttressed on the north by pre-Tertiary basement along the Leech River fault (Clowes *et al.*, 1987). Numerous faults occur in proximity to the terrane boundary in the eastern Strait of Juan de Fuca, the northern Puget Lowland, and the Cascade Range foothills (Johnson *et al.*, 2001; Mosher and Johnson, 2001), suggest that deformation occurs in a broad, distributed zone on many structures rather than on one discrete fault. In the northern Puget Lowland, other significant Quaternary structures within this distributed zone include the Devils Mountain fault, the Strawberry Point fault, and the Utsalady Point fault (Fig. 2) (Hobbs and Pecora, 1941; Loveseth, 1975; Gower *et al.*, 1985; Tabor, 1994; Johnson *et al.*, 2001).

The northwest-trending Utsalady Point fault, the subject of this report, was first recognized on the basis of offshore seismic-reflection profiles, faulted and folded Quaternary strata exposed in outcrops, stratigraphic offsets inferred from water-well logs, and high-resolution aeromagnetic surveys (Johnson *et al.*, 2001). This fault strikes obliquely across northern Whidbey Island, has a minimum length of 28 km, and forms the southern boundary of an uplifted block of pre-Tertiary basement rocks. Johnson *et al.* (2001) postulated oblique left-lateral slip for the Utsalady Point fault based on the near-vertical fault dip, reversals of throw along strike, evidence of associated contractional deformation, and the regional pattern of faults and folds mapped on seismic-reflection data. They suggested a minimum Quaternary vertical slip rate of about 0.15 mm/yr, but had no piercing points for estimating the lateral slip component.

Late Pleistocene Geology

During the latest Pleistocene Fraser glaciation (25 to 10 ka), the Puget Lowland and Strait of Juan de Fuca were occupied by lobes of the Cordilleran ice sheet. Retreat of Fraser ice, beginning about 16 ka (Porter and Swanson, 1998), was accompanied by rapid incursion of marine waters and isostatic rebound. Around northern Whidbey Island, the marine incursion began before about 13.6 ka and rebound-induced emergence was nearly complete by about 11 ka (Dethier *et al.*, 1995). During that ~13.6- to 11-ka interval, the Everson interstade, glaciomarine drift accumulated over much of the northern Puget Lowland. Domack (1982, 1983) and Dethier *et al.* (1995) described several distinct sedimentary facies and environments for the Everson glaciomarine drift, ranging from proximal (near ice), relatively massive deposits to more distal, well stratified beds. Sections of Everson drift commonly fine upward, reflecting increasing distance from the calving ice front. These sections commonly are overlain abruptly and erosionally by a coarse-grained, well stratified, "emergence facies," consisting of shallow-marine, beach, and estuarine beds deposited as isostatic rebound lifted former regions of glaciomarine environments through and above sea level. On northern Whidbey Island, the post-Fraser rebound has lifted glaciomarine deposits to elevations as high as 80 to 90 m above sea level (Dethier *et al.*, 1995).

Utsalady Point Fault Scarp

High-resolution "bald-earth" topography generated by an ALSM survey of Island County, Washington, shows a 1.4-km-long, 1- to 4-m-high, northwest-trending, southwest-

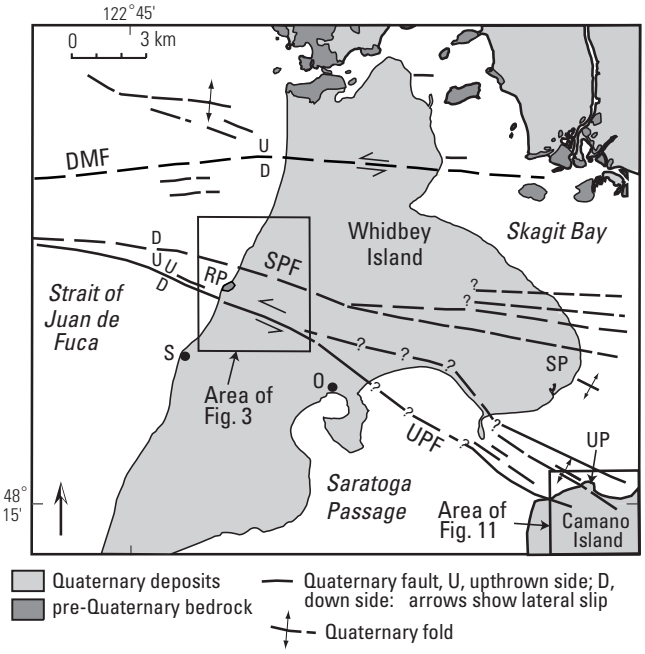

Figure 2. Map showing neotectonic setting of northern Whidbey Island, including area of Figures 3 and 11 (ALSM images). DMF, Devils Mountain fault; O, Oak Harbor; RP, Rocky Point; S, Swantown; SP, Strawberry Point; SPF, Strawberry Point fault; UP, Utsalady Point; UPF, Utsalady Point fault.

facing, topographic scarp (Fig. 3) that is coincident with the onshore projection of the Utsalady Point fault (Johnson *et al.*, 2001). The scarp extends across hummocky, low-relief, glacial terrain and has been locally modified by excavations for roads and a parking lot. Local variations in the scarp trend and short gaps in the continuity of the scarp coincide with inferred steps in the surface expression of the fault. We used the ALSM image and field reconnaissance to locate two trench sites, informally called "Duffers" and "Teeka," for paleoseismologic investigation (Johnson *et al*., 2003).

Teeka Trench

Teeka trench was excavated in the central part of a ~400-m-long section of the easternmost part of the scarp (Figs. 3 and 4). Scarp height at this location is approximately 300 cm. The lower part of the scarp (~6.3 to 12 m along the length of the trench) dips about 11.8°, which is markedly steeper than the ~6.6° slope of the upper part of the scarp (12 to 24 m along the trench length).

Trench Stratigraphy

Johnson *et al.* (2003) provide detailed maps of both the west and east (benched) walls of the Teeka trench (Figs. 4 and 5A). The trenches were mapped on digital photo mosaics and documented by using methods outlined by McCalpin (1996). Figure 4 shows a simplified map of the west wall. "Proximal" to "transitional" glaciomarine drift (Domack, 1982, 1983; Dethier *et al.*, 1995), consisting of a generally massive, silty clay diamict with scattered pebbles, is the lowest and oldest unit (unit 1) exposed in the trench. Three 1- to 2-m-deep, 1- to 3-m-wide, steep-sided channels (labeled A, B, and C) are incised into the unit 1 diamict. The channel

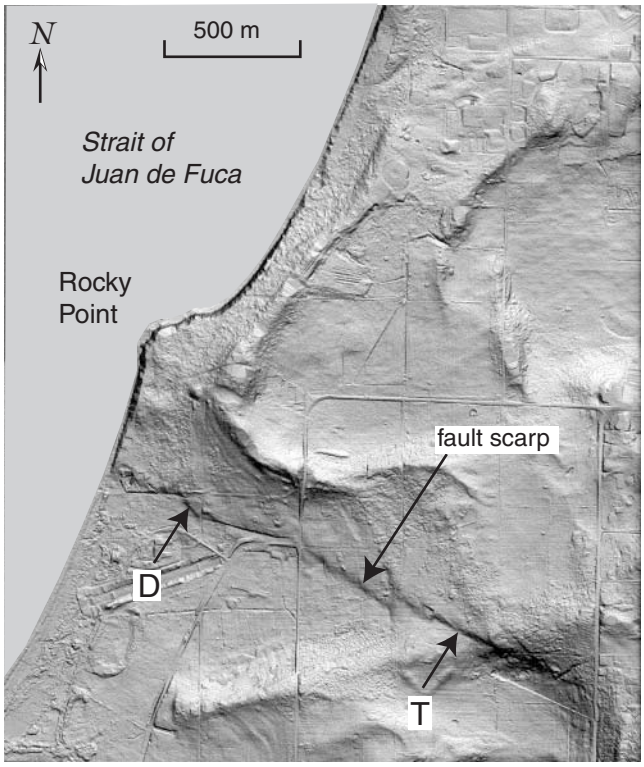

Figure 3. ALSM "bald-earth" image of Utsalady Point fault scarp on northwest Whidbey Island (Fig. 2), showing locations of the Duffers (D) and Teeka (T) trenches.

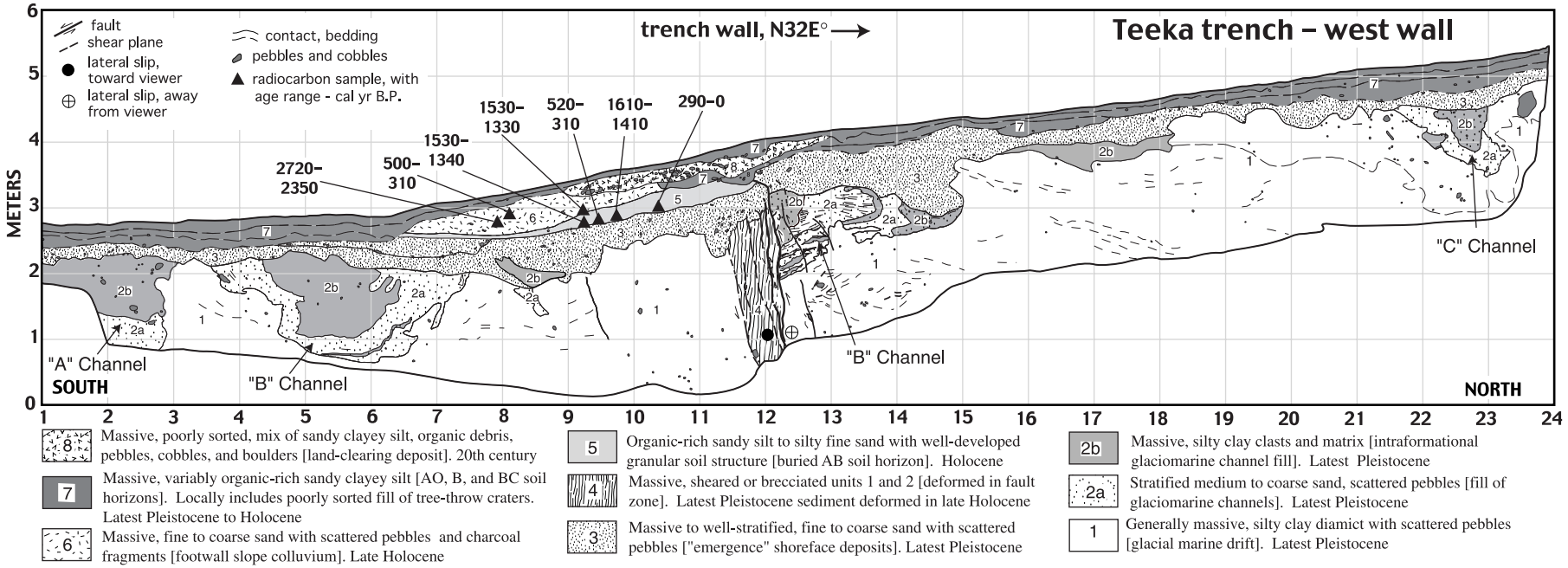

Figure 4. Map of the west wall of the Teeka trench, simplified from Johnson *et al.* (2003). Contacts within unit 7 separate three different soil horizons.

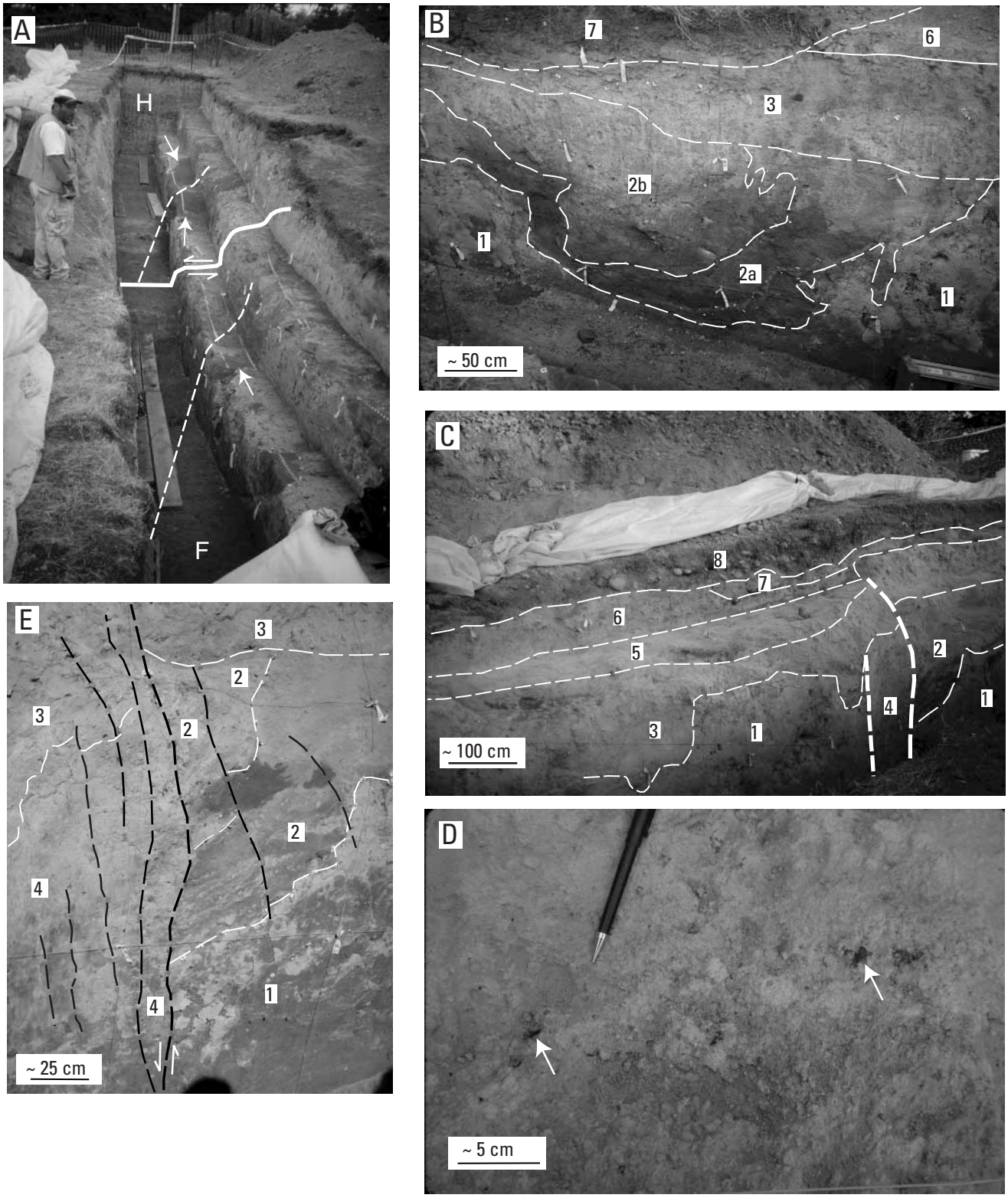

Figure 5. Photographs of the Teeka trench. Unit numbers are as in Figure 4. (A) View to the northeast, showing the benched east trench wall. Bold white line approximates trace of fault zone with half-arrows showing sense of lateral displacement. Dashed white line approximates axis of B channel axis used to estimate the amount of left-lateral slip (Fig. 6). White arrows show the location of both B channel margins in the hanging wall (two arrows) and the southern channel margin in the footwall (one arrow). "H" and "F" are on the fault hanging wall and footwall, respectively. (B) Exposure of B channel in the west wall of the trench between 4 and 8 m (Fig. 4). Dashed white line shows unit contacts. (C) West wall of the Teeka trench showing proximal part of the footwall, including fault zone (heavy dashed white lines), buried AB soil horizon (unit 5), and overlying scarp-derived slope colluvium (unit 6). (D) View of upper surface of unit 5 AB buried soil horizon with granular soil structure. Arrows show large charcoal fragments sampled for radiocarbon dating. (E) Fault zone (black dashed lines), showing truncation of B channel fill (unit 2) in the west wall. Arrows show vertical slip.

fills consist of well sorted sand (unit 2a) that is mixed with silty clay clasts and silty matrix (unit 2b) derived from adjacent channel walls (Fig. 5B). Domack (1982) suggested that such channels were cut by dense, sediment-charged currents in proximal to transitional glaciomarine environments. The trends and geometry of the three channels were determined by mapping and high-precision electronic distance meter (EDM) surveys (Fig. 6).

Unit 3 overlies units 1 and 2 along a gentle to locally steep erosional unconformity (Fig. 5C). Unit 3 is a sheet-like body of massive to horizontal- or low-angle bedded, moderately to well sorted, fine to coarse sand with scattered pebbles. This stratigraphic relationship (bedded pebbly sand above massive glaciomarine deposits) has been described at numerous locations in the northern Puget Lowland (e.g., Domack, 1982; Dethier *et al.*, 1995), with the upper unit interpreted as "emergence" beach and shoreface facies. Unit 4 is glaciomarine drift (units 1 and 2) that has been sheared and deformed in the fault zone. The shearing in unit 4 also extends upward into unit 3; however, discrete shear planes are less distinct in this unit because of its sandy lithology.

Unit 5 is an organic-rich AB soil horizon having granular structure, consisting of sandy silt to silty fine sand and scattered charcoal fragments (Fig. 5C, D). This unit is clearly distinguished only on the footwall of the fault between 6.5 and 12 m in the trench, where it is buried by overlying strata (Fig. 4). Unit 5 correlates with unit 7 in the upper and lower parts of the trench. It is distinguished as a separate stratigraphic unit solely on the basis of its burial below overlying colluvium.

Unit 6 overlies unit 5 and consists of massive, fine to coarse sand with scattered pebbles and rare charcoal fragments (Figs. 4, 5C, D). Unit 6 lacks soil structure and is interpreted as scarp-derived slope colluvium derived from erosion of unit 3 and the lower part of unit 7.

Unit 7 is massive, variably organic-rich, sandy, clayey silt with scattered pebbles (Fig. 4). This unit represents latest Pleistocene to Holocene soil and varies in character across the trench due to the effects of faulting, slope, and soil-forming processes. The upper part of unit 7 is an AO soil horizon with granular structure consisting of a mat of grass roots mixed with sandy clayey silt. The middle part of unit 7 is a Bw soil horizon consisting of pervasively rooted, sandy clayey silt with subangular blocky structure. The lower part of unit 7 is a BC horizon formed by weathering of unit 3; it consists of silty to medium sand and sandy clayey silt with scattered pebbles, is weakly cemented, and has weak, irregular, subangular, blocky structure. Unit 7 also locally includes a poorly sorted mix of sandy silt, pebbles, soil clasts, and organic debris filling gentle concave-upward depressions, most notably between unit 8 between 10.5 and 12.1 m along the trench. These deposits were broken out as a separate unit in more detailed trench logs (Johnson *et al.*, 2003) and are interpreted as the fill of tree-throw craters. Unit 7 is notably thinner and less well developed in the middle of the trench (steepest part of scarp) where it overlies units 6 and 8.

Unit 8 is a lense of organic-rich, massive, poorly sorted, sandy, clayey silt, organic debris, pebbles, cobbles, and boulders, occurring locally near the base of the scarp (Figs. 4, 5C). This mixed unit is a human-formed deposit of glacial erratics and other large clasts produced when the land was cleared for dairy farming in the early to mid-twentieth century. Unit 8 is overlain by the upper soil unit (AO horizon) of unit 7.

Evidence for Holocene Deformation

A northwest-striking (~305°) fault, parallel to the scarp, offsets latest Pleistocene units 1, 2, and 3 in the central part of Teeka trench both vertically and horizontally (Figs. 4, 5E) (Johnson *et al*., 2003). On the west trench wall, the fault is represented by a near-vertical primary fault and a 60-cm-wide zone of sheared and tectonically mixed units 1 and 2 (unit 4). The primary fault sharply truncates the unit 2 fill of the "B" glaciomarine channel and vertically displaces the

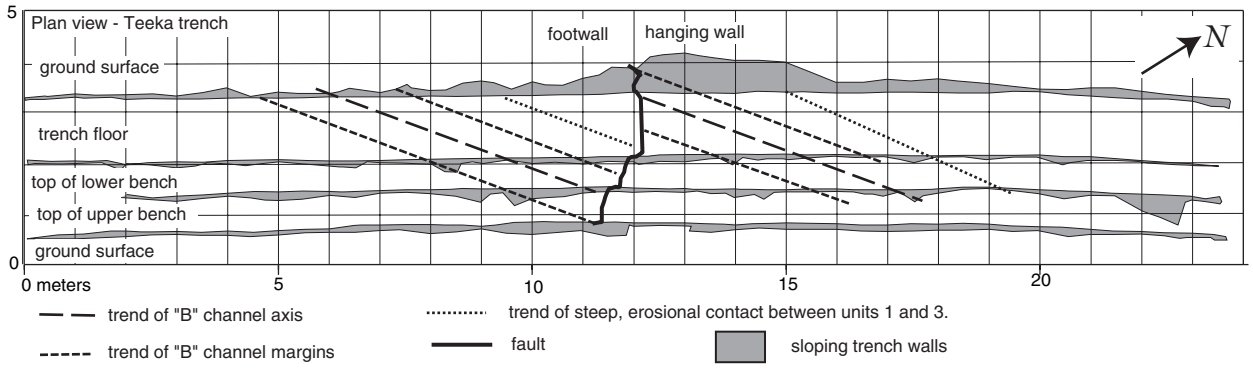

Figure 6. Plan-view (vertical) map of the Teeka trench based on the EDM survey, showing trends of piercing points used to document the amount of left-lateral slip on the fault. Piercing points include B channel axis and margins (Figs. 4, 5), and the steep erosional contact between units 1 and 3 (e.g., between 9 and 10 m in Fig. 4).

lower contact of unit 3. The primary fault and related shears are less distinct in unit 3 because of its more friable and sandy texture.

Both vertical (up to the northeast) and left-lateral slip are inferred for the fault zone. On the west trench wall, contacts between units 1, 2, and 3 directly adjacent to the fault are erosional and thus are not ideal stratigraphic markers for estimating offset. Based on the stratigraphy a few meters away from the fault zone where the contacts are relatively flat, we estimate that the vertical separation of the lower contact of unit 3 is approximately 115 ± 20 cm. On the east wall of the trench, vertical separation is approximately 130 ± 20 cm.

Estimates of left-lateral slip are based on correlation of the "B" channel fill (unit 2) between the hanging wall and footwall (Figs. 4, 5A, B). This correlation is based on the strong similarity of channel depth, width, and shape, the parallel trends of the channel axes and margins, and the identical lithologic character and internal architecture of the channel fill. In the hanging wall, the B channel is completely exposed in the east trench wall but only partly exposed because of fault truncation in the west wall. In the footwall, the B channel is completely exposed in the west wall but truncated in the east wall. The absence of the channel on opposite sides of the fault on both trench walls is compelling evidence of lateral slip. If motion on the fault was strictly vertical, then the channel would be present on both sides of the fault in both trench walls.

A high-precision EDM survey of the B channel axis and margins (Fig. 6) reveals that, in the hanging wall, the northern margin of channel B trends 53°, which is 21° more northeast than the trend of the trench. In the footwall, the southern margin of the channel and the channel axis trend 51° and 53°, respectively. Projecting the trends of the channel axis and margins beyond the trench, then restoring them to make a continuous channel, yields an estimate of 200 to 220 cm of left-lateral slip.

We attribute the fault-related deformation in the Teeka trench to one earthquake. In this event, vertical movement raised and laterally shifted the hanging wall, exposing units 3 and 7, which provided a source for unit 6 colluvium. Deposition of the colluvial wedge buried the soil (unit 5) on the downdropped footwall. The presence of a single buried soil and colluvial wedge in the footwall suggests that only one postglacial ground-rupturing earthquake occurred at this site. Net slip on the fault during this event, determined by summing the minimum and maximum lateral and vertical components described above, was about 220 to 265 cm.

Time of Faulting

Radiocarbon ages (Table 1) of charcoal fragments present in the unit 5 buried soil (four ages) and the unit 6 scarp-derived colluvium (three ages) constrain the time of the ground-rupturing earthquake. The charcoal is assumed to have formed during local forest fires. We consider the ages as one group because of their common genetic linkage to the fault-related deformation (see previously). Three ages are between 520 and 0 cal yr B.P., three ages are between 1610 and 1330 cal yr B.P., and one age is between 2720 and 2350 cal yr B.P. Two scenarios seem possible given the ages. In the first, the younger suite of ages provides a close maximum age for burial of the soil by colluvium and hence the time of the earthquake. In this scenario, older charcoal was at or near the surface for as much as a few thousand years prior to the earthquake. Charcoal that is thousands of years old is common in soils of forested landscapes in the Pacific Northwest (Gavin, 2000; Nelson *et al.*, 2003).

In the second scenario, the suite of ages between 1610 and 1330 cal yr B.P. provides the maximum age for the earthquake, and the three younger ages are from burned roots or were infiltrated into root casts, burrows, or soil fractures. There is no field evidence to support the infiltration hypothesis, however, and the large size of the three charcoal samples that gave the youngest ages (Table 1) is similarly inconsistent with infiltration. Moreover, evidence for significant vertical sediment mixing, such as disturbed unit contacts or distinct burrows, which might obscure the origin of infiltrated charcoal, is also lacking. Given this field evidence and the presence of charcoal of the same age and in the same stratigraphic context in Duffers trench (Table 1; Figs. 7, 8), we consider the second scenario highly unlikely.

Evidence for Prefaulting Deformation

There are three possible explanations for the discrepancy between vertical separation across the fault (95 to 150 cm) and scarp height (300 cm) at the Teeka trench: (1) Folding occurred during the most recent earthquake; (2) folding occurred during an earlier postglacial earthquake not characterized by ground rupture; or (3) some of the separation is related to primary postglacial depositional dip (4° to 5°) associated with a postglacial emergence shoreline. The latter hypothesis is unlikely because of the low probability that the scarp is exactly coincident with the unit 3 shoreline, the scarp linearity and short wavelength are inconsistent with other nearby emergence shorelines, and there is no topographic rise behind the scarp that could be interpreted as a shoreline back edge (Fig. 3). Either of the first two hypotheses are viable; we favor folding during an earlier postglacial earthquake because of the lack of evidence for shortening in the Teeka fault zone (Fig. 4) and because our interpretation of deformation in Duffers trench favors two late Holocene earthquakes (see following text).

Duffers Trench

Duffers trench was excavated in the middle of a ~80-m-long, northwest-trending step at the west end of the scarp (Fig. 3). Scarp height at this site is approximately 430 cm. The average dip of the scarp is about 8°, but it is as steep as 19° above the fault in the southwest part of the trench.

Table 1
Radiocarbon Data for Samples from Trenches Crossing the Utsalady Point Fault

Sample No.	Unit No.	Station (m)*	Radiocarbon Lab. No.†	Lab Age (^{14}C B.P. at 1 σ)‡	Calibrated age (cal yr B.P. at 2σ)§	Sample weight (mg)‖	^{13}C (‰)	Description of Dated Charcoal‖
Duffers trench								
DF-23	6	2.49, 3.03	Beta-170979	460 ± 40	550–330	54.8	−23.8	5 × 8 × 3 mm fragment
DF-39	6	3.78, 3.19	Beta-172552	380 ± 40	510–310	48.2	−26.2	8 × 6 × 4 mm fragment
DF-40	6	0.65, 2.80	Beta-172551	330 ± 40	490–300	40.9	−25.1	13 × 5 × 5 mm fragment
DF-10	5b	9.41, 3.75	Beta-174108	3150 ± 40	3470–3260	46.6	−25.0	10 × 5 × 4 mm fragment
DF-14	5b	9.45, 3.69	Beta-170977	3110 ± 40	3450–3210	125.0	−24.8	4 × 3 × 2 mm fragment
DF-16	5b	7.82, 3.90	Beta-170978	1280 ± 40	1290–1080	80.6	−25.2	Part of 30 × 100 mm root
DF-21	4a	6.65, 3.47	Beta-172554	1330 ± 40	1310–1170	20.6	−24.0	20 × 40 × 10 mm fragment
DF-27	4a	2.40, 2.82	Beta-170980	310 ± 40	470–290	28.4	−25.6	4 10 × 10 × 10 mm pieces
DF-13	4c	9.53, 4.05	Beta-172553	1220 ± 40	1270–1050	71.2	−23.9	6 × 6 × 5 mm fragment
DF-18	4c	7.87, 3.41	Beta-174109	3380 ± 40	3720–3470	69.2	−25.8	10 × 12 × 8 mm fragment
DF-58	4b	9.11, 3.51	Beta-170981	2170 ± 40	2330–2040	160.0	−22.2	17 × 17 × 2 mm fragment
Teeka trench								
T-36	5	10.40, 3.00	Beta-170982	160 ± 40	290–0	60.5	−23.9	Part of 5 × 10 × 10 mm fragment
T-39	5	9.30, 2.85	Beta-172555	1550 ± 40	1530–1340	76.3	−24.9	Charred flaky wood, possibly bark; part of 30 × 50 × 1 mm mat
T-45	5	9.68, 2.90	Beta-170984	1620 ± 40	1610–1410	38.0	−25.4	Part of 40 × 40 × 10 mm fragment
T-46	5	9.50, 2.90	Beta-170985	400 ± 40	520–310	113.9	−22.9	Part of 20 × 10 × 5 mm fragment
T-40	6	9.17, 2.96	Beta-170983	1540 ± 40	1530–1330	89.4	−25.3	Flaky, part of 8 × 5 × 1 mm fragment
T-42	6	8.12, 2.90	Beta-172556	350 ± 40	500–310	63.2	−25.2	Part of 15 × 10 × 5 mm fragment
T-44	6	7.85, 2.80	Beta-172557	2450 ± 40	2720–2350	55.3	−25.6	Part of 20 × 10 × 5 mm fragment

*Location (horizontal, vertical) on reference grid used to map the northwest wall of each trench.

†Laboratory: Beta Analytic, Inc., Miami, Florida.

‡Quoted error for each AMS (accelerator mass spectrometer) analysis is the larger of counting error or target reproducibility error.

§Ages in calibrated (approximate solar) years calculated using OxCal (version 3.4, Bronk Ramsey, 1998; probability method) and the INTCAL98 dataset of Stuiver *et al.* (1998). Beta Analytic, Inc., states that no additional laboratory variance (error multiplier; e.g., Taylor *et al.*, 1996) need be added to ages for calibration. Calibrated ages show intervals of >95% probability distribution at 2σ.

‖Unless indicated otherwise, ages are on angular, unabraded fragments of charcoal with distinct wood cellular structure. For each sample, the largest, most angular, least decayed fragments of charcoal were selected to minimize the chance of analyzing carbon much older than the host sediment. Sediment adhering to fragments was removed with brushes or dental tools in distilled water using a dissection microscope at 6 to 25×. Charcoal was picked directly from sediment collected from the trench wall.

Trench Stratigraphy

Figure 7 shows a simplified map of the west wall of Duffers trench, and Figure 8 shows a more detailed but still simplified map of the fault zone in the central part of the trench. More detailed maps are in Johnson *et al.* (2003).

Unit 1 consists of distal glaciomarine drift (Domack, 1982, 1983; Dethier *et al.*, 1995). Strata are well stratified, interbedded to laminated silt and clay with thin sand beds and partings (Fig. 9A). Abundant graded bedding indicates deposition primarily by turbidity currents. Randomly scattered pebbles as large as 15 cm in diameter are interpreted as dropstones. Convolute lamination is common. Based on lithology and stratigraphic position, Johnson *et al.* (2003) defined several subunits within unit 1, which we easily traced across the length of the trench. Marker beds within subunit 1a are shown as the marker beds "a" through "e" on Figures 7 and 8. The upper part of unit 1 is locally mottled, is intruded by roots, and has weak prismatic soil structure.

Unit 2 consists of stratified to massive pebbles, granules, sand, and silty sand deposited unconformably on unit 1. Like unit 3 in the Teeka trench, unit 2 was deposited in a shoreface environment as the land surface isostatically rebounded through sea level after glacial retreat. Duffers trench is about 30 m lower than the elevation of Teeka trench, so the Duffers "emergence facies" were deposited after those at the Teeka site during the rebound-induced regression. Unit 2 is thickest in the lower and upper parts of the trench and is locally absent from the steepest part of the scarp in the middle of the trench because of uplift-induced erosion.

Unit 3 in the Duffers trench is similar to unit 4 in the Teeka trench in that it consists of glaciomarine drift that was sheared and deformed in a fault zone.

Unit 4 consists of massive, locally iron-stained and root-stirred, gravel, granular sand, and silty sand. This unit is present only in the lowest part of the trench where it is inferred to be a soil developed on unit 2 and then buried by units 5 and 6 (Fig. 9B).

Unit 5 is a heterogeneous mixture of locally cemented, massive, pebbly silty sand and clay with variably developed soil structure. Unit 5 is present only in the trench fault zone and in the footwall of the fault. Different subunits of unit 5 are interpreted as scarp-derived colluvium, hanging-wall

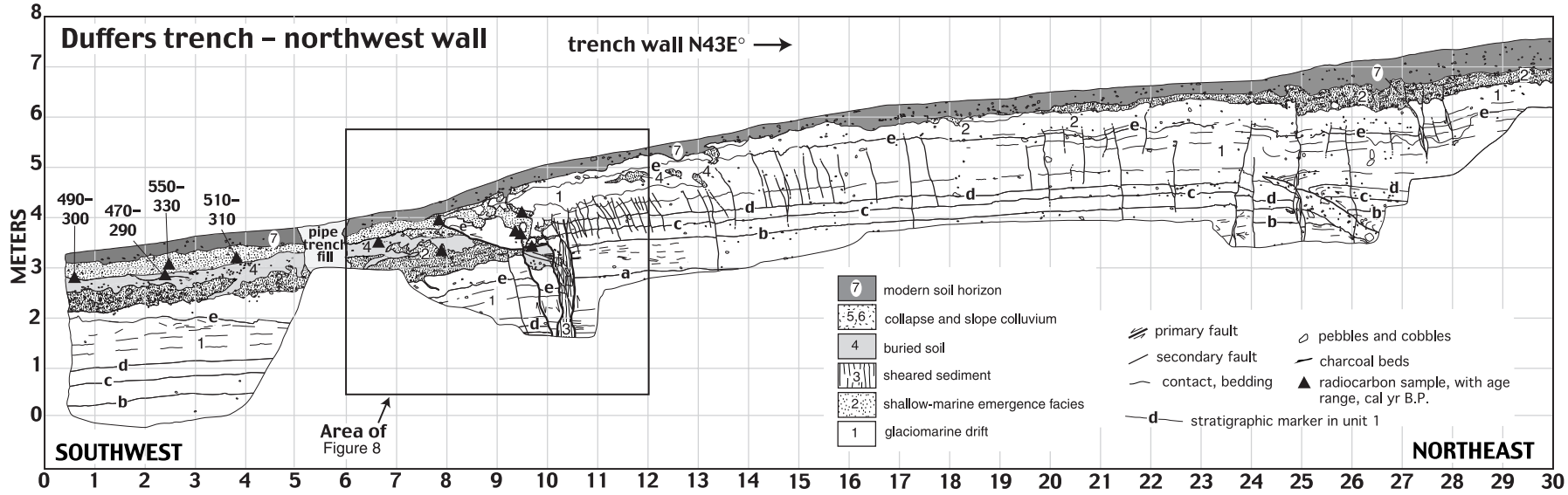

Figure 7. Map of the west wall of the Duffers trench, simplified from Johnson *et al*. (2003). Detailed unit descriptions and large-scale view of fault zone are shown in Figure 8.

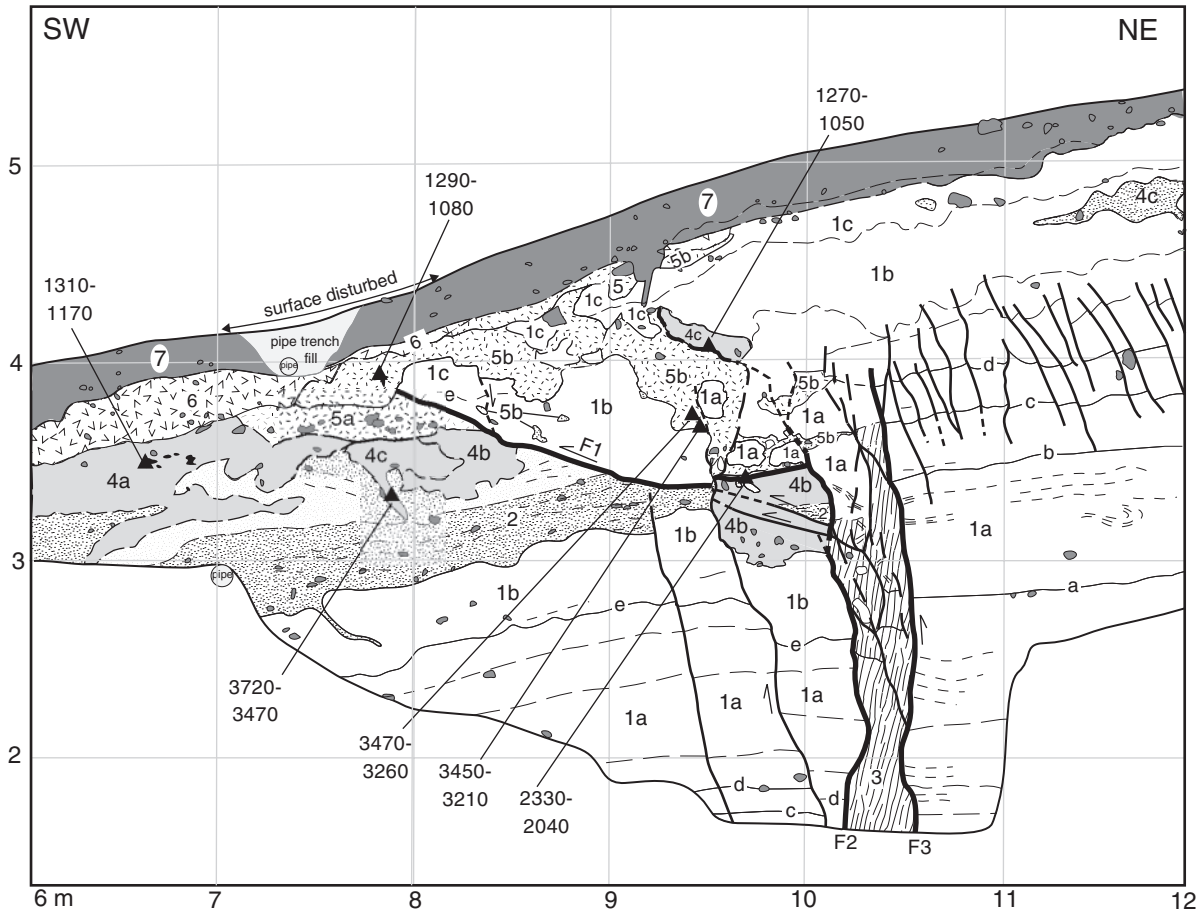

7 - Massive, pebbly to silty sand and sandy silt [root-stirred AB and B horizons]. Latest Pleistocene to late Holocene.

6 - Massive, pebbly, silty sand [root-stirred slope colluvium, buries unit 4 soil; occurs on and below base of scarp formed by collapsed hanging wall]. Common argillic Bt horizon. Late Holocene.

5b - Massive, pebbly silty clay to silty sand [hanging-wall-collapse colluvium and fill of extensional hanging-wall fissures]. Local well-developed Bt horizon and (or) silica cementation. Late Holocene.
5a - Heterogeneous mixture of weakly silica(?)-cemented sediment derived from units 1 and 2; [hanging-wall collapse colluvium lying beneath and southwest of thrust tip]; has weak, discontinuous B horizon. Late Holocene.

4c - Root casts filled with sediment of units 1 and 2 and organic matter. Late Holocene.
4b - Massive, dark gray to black, organic-rich sand [root-stirred remnants of buried A soil horizons]. Present in fault zone and was deformed by faulting. Latest Pleistocene to late Holocene.
4a - Massive, iron-stained gravel, sand, sandy gravel, and silty sand [soil, weakly developed on unit 2; locally buried or developed on unit 5]. Latest Pleistocene to late Holocene.

3 - Sheared sediment of units 1 and 2 [deformed by slip on faults F4 and (or) F5]. Latest Pleistocene strata deformed in the late(?) Holocene.

2 - Stratified to massive pebbles, gravel, sand, and silty sand; unconformably deposited on unit 1 [beach and shoreface deposits, related to postglacial rebound and emergence]. Latest Pleistocene, about 14-15 ka.

1c - Clayey silt and silty clay with prismatic soil structure; weak Bt soil horizon developed in unit 1.
1b - Massive upper part of unit 1, characterized by prominent orange, iron-stained mottling and root casts.
1a - Interbedded silty clay, silt, sand, and pebbly sand; common graded beds, soft-sediment deformation structures, and dropstones [glacial marine drift, mainly deposited by turbidity currents]. Distinct marker horizons designated by "a," "b," "c," "d," and "e." Latest Pleistocene, about 15 ka.

Figure 8. Central part of the Duffers trench, showing the main fault zone. Explanation of symbols is in Figure 7. Simplified from Johnson *et al*. (2003).

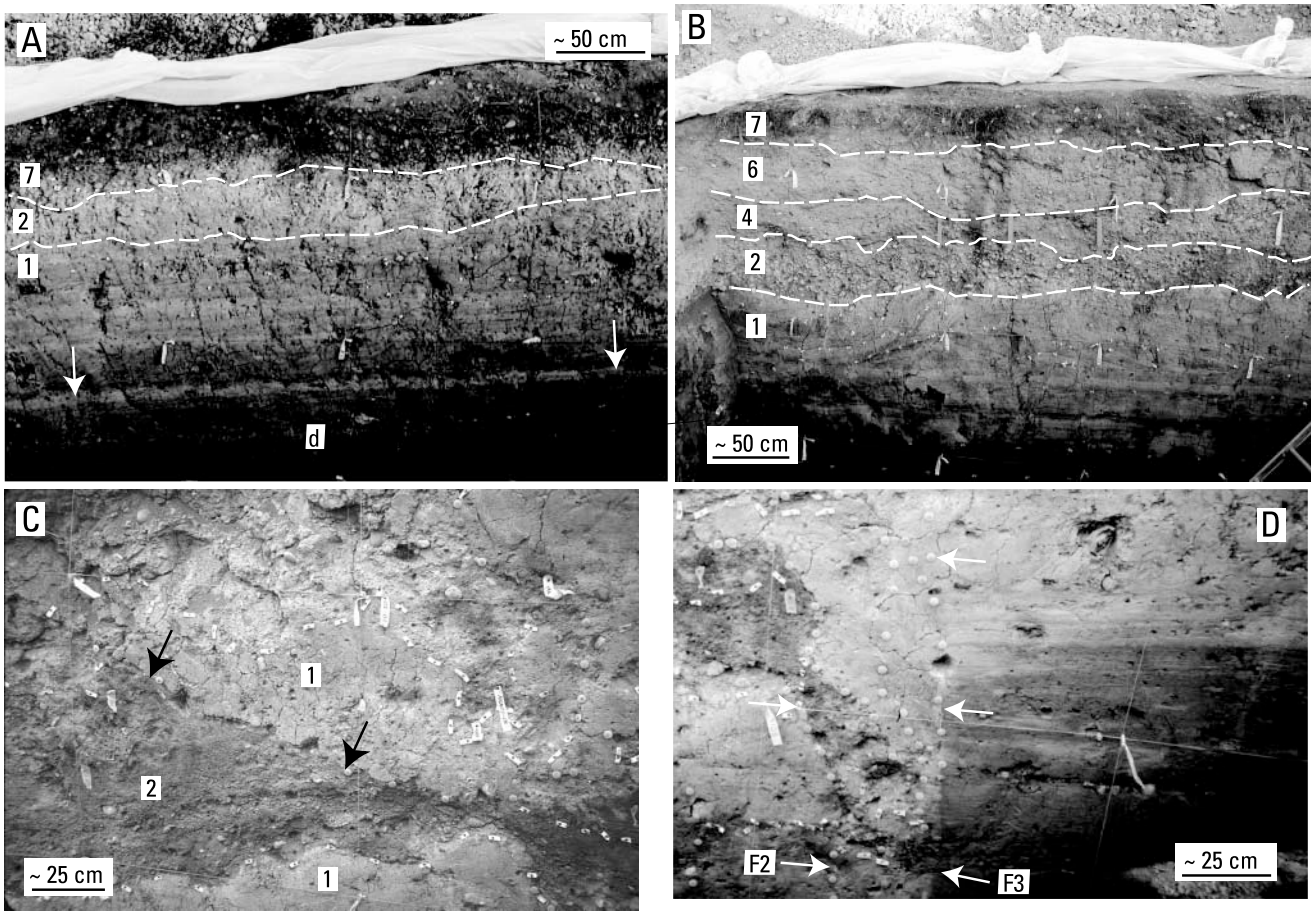

Figure 9. Photographs of the Duffers trench northeast wall. Numbers represent units as shown in Figures 7 and 8. (A) Upper part of trench (centered on meter 18) showing well defined stratigraphy within unit 1. White arrows identify prominent continuous bed above marker "d" (Fig. 7). (B) Stratigraphy in lowest part of trench, showing fine-grained glaciomarine drift (unit 1), pebbly shoreface sand (unit 2), buried soil (unit 4), slope colluvium (unit 6), and the modern AB horizons (unit 7). Dashed white lines are unit contacts. (C) Subhorizontal fault F1 (arrows), with unit 1 thrust over unit 2 (Fig. 8). Location is between meters 3 and 4 (vertical) and meters 8 and 9 (horizontal). (D) Subvertical faults F2 and F3 (white arrows), which truncate marker beds in unit 1

collapse colluvium, and fill of extensional fissures (Fig. 8). Unit 6 is a massive, pebbly, silty sand interpreted to be scarp-derived slope colluvium.

Unit 7 is massive, root-stirred, variably organic-rich and cemented, pebbly to silty sand and sandy silt. Unit 7 blankets the trench and includes AB and Bw and (or) Bt soil horizons. The unit is thickest and the soil structure is best developed in the upper part of the trench. Unit 7 in the hanging wall correlates with both units 4 and 7 in the footwall.

Evidence for Holocene Deformation

Strata in the Duffers trench are cut by numerous faults and fractures, but the largest stratigraphic offset is in the main fault zone centered on meter 10 near the base of the scarp (Figs. 7, 8, 9C, D). Vertical separation on the "d" marker of unit 1 across the fault is about 2.1 m. By comparison, vertical separation of stratigraphic markers across the entire 4.3-m-high scarp varies from about 3.7 m (marker "d") to about 4.5 m (base of unit 2).

Most displacement across the zone occurs on two sets of structures. Fault F1 and related low-angle structures dip ~20° to the northeast (Figs. 7, 8, 9C) and thrust unit 1 over unit 2. Faults F2 and F3 are near-vertical structures that appear to truncate F1 (Figs. 7, 8, 9D).

Figure 10 shows one scenario of faulting, inferring two ground-rupturing earthquakes. Figure 10A shows a prefaulting stratigraphy consisting of units 1 and 2, the overlying soil, and a future fault plane. Figure 10B postulates that fault F1 was continuous with the lower parts of faults F2 and F3, on which 110 cm of vertical slip is restored. During faulting, a large extensional fissure forms in the hanging wall above the prominent bend in the fault, and a small amount of hanging-wall collapse colluvium was overridden near the

(Fig. 8). Location is between meters 10 and 11.

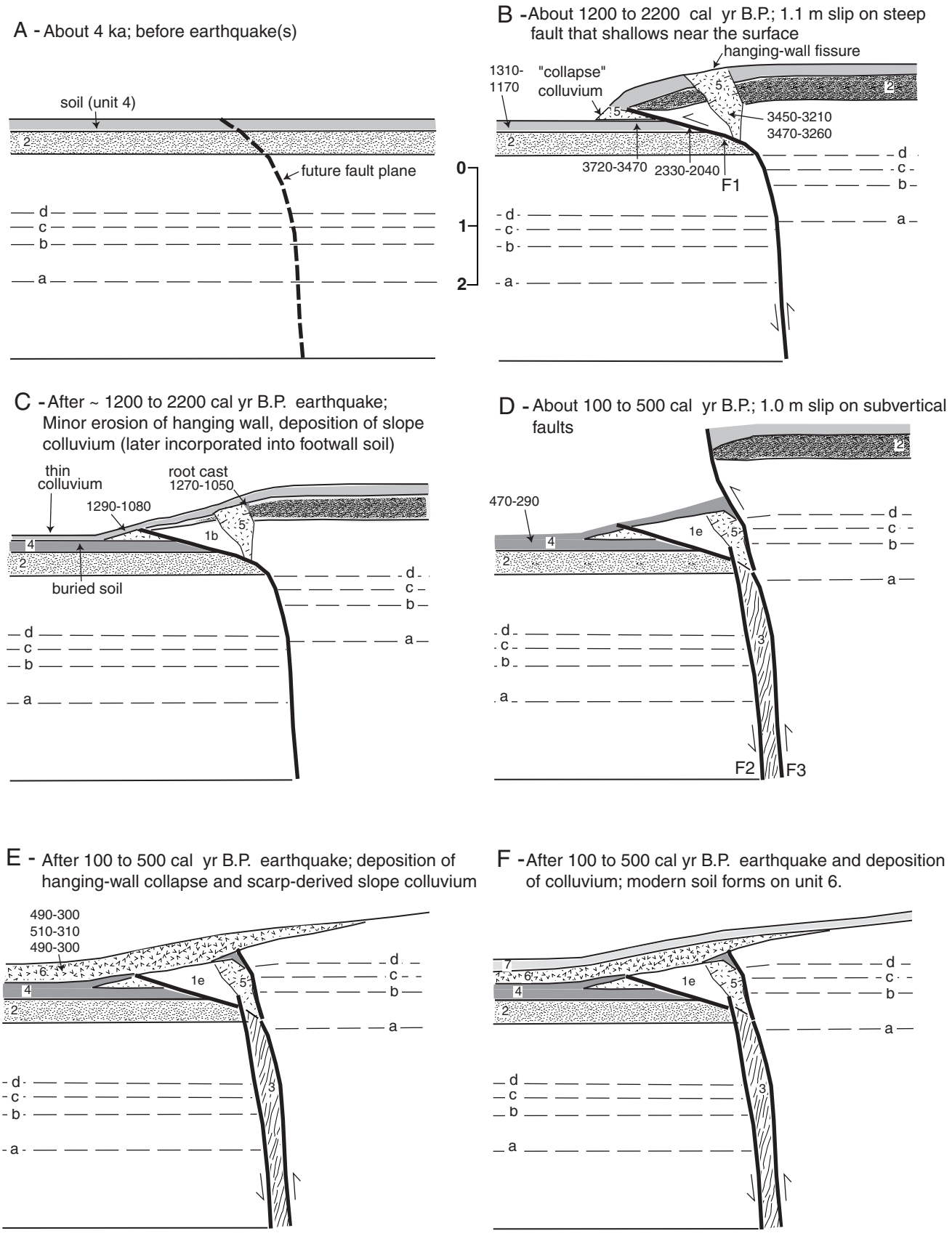

Figure 10. Schematic diagram showing the deformation history for a two-earthquake scenario in the Duffers trench on the Utsalady Point fault. Numbers refer to units shown on Figures 7 and 8. Calibrated radiocarbon ages (Table 1; 2σ) are shown as range in cal yr B.P. (e.g., 2330 to 2040).

fault tip. Because of the near-surface shallowing of the fault, a significant free face did not exist at the surface. Unit 5 ages from charcoal in the fissure fill are 3450 to 3210 and 3470 to 3260 cal yr B.P. Charcoal from the soil beneath the "fault-tip colluvium" (unit 4c) was dated at 3720 to 3470 cal yr B.P., and charcoal from a sheared A horizon beneath the hanging wall (unit 4b) was dated at 2330 to 2040 cal yr B.P. (Fig. 10D).

After this faulting event, unit 2 and overlying soil were eroded from the uplifted, proximal part of the hanging wall to produce a small amount of slope colluvium that was subsequently incorporated into the footwall soil (Fig. 10C, D). Charcoal fragments from this colluvium or from soil developed on this colluvium yielded ages of 1310 to 1170 and 1290 to 1080 cal yr B.P. A charcoal fragment in a large root cast (unit 4C) inferred to merge with the displaced soil horizon along the upper part of the fault zone yielded an age of 1270 to 1050 cal yr B.P.; presumably this root cast formed in a weak zone created by extension in the fault hanging wall.

In Figure 10D, 1.0 m of slip on the subvertical F2-F3 faults occurred during a second earthquake, with negligible slip on F1. The faulting created a steep scarp, which provided a source for both hanging-wall collapse colluvium and the scarp-derived colluvium that buries the footwall soil (Fig. 10E). The steepness of the scarp compared with that which formed in the first earthquake (Fig. 10B) is attributed to the increased presence of cohesive, fine-grained unit 1 in the hanging wall. The upward continuation of faults and shears in the F2-F3 zone is probably greater than shown in Figure 8, but difficult to map due to the intense weathering and root stirring of the homogeneous silty clay (lacking marker beds) of the upper part of unit 1. Fault F3, which bounds the northeast side of unit 5B (Fig. 8), was probably the main fault. A charcoal fragment from the buried footwall soil yielded an age of 470 to 290 cal yr B.P., and three charcoal fragments from the unit 6 slope colluvium yielded ages of 490 to 300, 510 to 310, and 550 to 330 cal yr B.P. After the second faulting event, a soil formed over the proximal fault footwall and hanging wall (Fig. 10F).

Faulting can thus be schematically restored in the Duffers trench using well constrained vertical stratigraphic offsets. However, given the strong evidence for strike-slip offset at Teeka trench, it is probable that there is also a component of lateral slip on the Duffers trench fault zone. Simplified two-dimensional restorations of faulting (e.g., Fig. 10) are thus likely to be incomplete, however, they can provide an approximation for the vertical component of faulting and a plausible basis for inferring an earthquake history.

Approximately 90 cm of the 160 to 240 cm of vertical separation not accommodated on the master fault zone in the Duffers trench is taken up by gentle folding in the fault footwall (Fig. 7). Stratigraphic markers in the footwall adjacent to the fault zone dip as steeply as 11° to 15°, but these dips shallow to about 4° at the southern end of the trench. The remaining ~70 to 150 cm of vertical separation in the trench is accommodated by folding and associated subvertical bending-moment faulting in the hanging wall (Fig. 7). The average dip of stratigraphic markers in this part of the trench is about 2°.

The trench map also shows a low-angle fault in the upper part of the trench (m 25–26) (Fig. 7). This fault is interpreted as a soft-sediment deformational structure, probably associated with sudden subaqueous loading by a sediment gravity flow or iceberg dumping. The fault dies out in unit 1 and is cut by the younger subvertical bending-moment faults.

Time of Deformation and Number of Earthquakes

The sequence of faulting outlined in Figure 10 first shows slip on a vertical fault that rolls over to a subhorizontal fault near the surface. The subhorizontal fault is truncated by later vertical slip on the same zone. In Figure 10, we propose an interpretation in which the two styles of faulting are separated in time; however, it also possible that faulting in the trench records two different phases of movement during a single event.

We favor the two-event hypothesis because of the distribution of radiocarbon ages and the complex crosscutting fault relationships (Fig. 8). The three oldest ages (3720 to 3210 cal yr B.P.) (Table 1; Figs. 8, 10) are from unit 5 samples located in a hanging-wall fissure, or from colluvium generated in the first of two events or in the early phase of a single event. A fourth age (2330 to 2040 cal yr B.P.), from a large charcoal fragment in a sheared AO soil horizon below fault F1 (Table 1), provides a maximum age for the first faulting event. The numerous detrital charcoal ages in the range of about 1600 to 1100 cal yr B.P. from both the Duffers and Teeka trenches provide the basis for estimating a minimum age for this first event. These ages suggest that one or more large forest fires occurred during that time. If the first earthquake occurred after these fires, then the fill of the Duffers hanging-wall fissure (unit 5b) (Fig. 8) would likely contain charcoal fragments of this age. Because it does not suggests that the inferred penultimate earthquake occurred before about 1200 cal yr B.P.

Charcoal in the buried soil (unit 4) in the footwall yielded three ages of 470 to 290, 490 to 300, and 1310 to 1170 cal yr B.P., and charcoal from the overlying colluvium (unit 6) yielded ages of 510 to 310, 550 to 330, and 1290 to 1080 cal yr B.P. Hence, the most recent earthquake occurred after about 300 to 500 cal yr B.P. and is inferred to correlate with the large-slip earthquake recorded in the Teeka trench.

In the single earthquake hypothesis, movement would occur as successive phases during the same event, and the "in-sequence" series of ages, which fits the two-earthquake hypothesis so well, would be entirely coincidental. In this single-event scenario, older charcoal would have to be near the surface for as long as 3000 years before being buried by colluvium or deposited in a fissure during or shortly after a

post-~500 cal yr B.P. earthquake. Factors that favor this single-event interpretation include the absence of unequivocal stratigraphic evidence for a second large Holocene earthquake in the Teeka trench and the absence of a second buried soil and colluvial wedge in the Duffers trench footwall. The missing second buried soil and colluvial wedge, however, can be explained by the first event producing only a small amount of colluvium because of the shallow, near-surface dip of fault F1, and the incorporation of first-event colluvium into unit 4 buried soil. Although we can not preclude the single-event scenario, we favor the interpretation of two distinct ground-rupturing events based on the combined evidence from both trenches.

Discussion

Earthquake History of the Utsalady Point Fault

Two trenches on northern Whidbey Island provide evidence of at least one and probably two large late Holocene earthquakes on the Utsalady Point fault. Radiocarbon ages from buried soils and overlying colluvium in both trenches indicate that the most recent earthquake occurred sometime after about A.D. 1550 (400 cal yr B.P.). The historic catalog of large earthquakes in this part of the Pacific Northwest (Ludwin and Qamar, 1995), which extends back to about A.D. 1850, does not mention such an event, so we think this earthquake occurred between about A.D. 1550 and 1850. Given this recency, it is possible that this earthquake might be part of local native American lore (e.g., Ludwin, 1999); however, as of yet, no prehistoric account of such an earthquake has been discovered. The Duffers trench contains evidence that favors a second earlier earthquake, which occurred between about 2200 and 1100 cal yr B.P. If this earthquake did occur, it probably caused folding but not faulting at the Teeka trench locality.

Johnson *et al.* (2001) suggested left-lateral transpression on the Utsalady Point fault based on regional deformation patterns, a hypothesis that is supported by the laterally offset channel deposits in the Teeka trench. Given left-lateral slip, the right bend in the scarp at the Duffers trench site would be a restraining bend in the fault zone (e.g., Christie-Blick and Biddle, 1985), which is consistent with a large amount (~ 2 m) of late Holocene contractional folding at the locality.

In the two-earthquake scenario, the two earthquakes appear to have somewhat different deformation styles. The most recent event was characterized predominantly by the left-lateral slip at Teeka trench compared with the mainly vertical offset with a probable strike-slip component at the Duffers trench. Deformation during the penultimate earthquake is inferred to have a shortening component, involving faulting and folding at the Duffers trench and folding at the Teeka trench.

Johnson *et al.* (2001) previously suggested that earthquakes of $M \geq \sim 6.7$ were possible on the Utsalady Point fault given its minimum length (25 km) and the empirical relation between rupture length and earthquake magnitude defined by Wells and Coppersmith (1994). The rupture length for the last earthquake is not known, but the onland portion of the scarp is only about 1.4 km long (Fig. 3). The scarp's short length relative to minimum length and the amount of fault slip determined in the trenches suggests several possibilities: (1) ground rupture was limited, (2) the scarp has been degraded beyond recognition by slope processes or urban development, (3) slip on the fault was mostly strike-slip with minimal vertical displacement, (4) the amount of relief along much of the fault is below the detection level of ALSM, or (5) surface rupture extends well offshore in the eastern Strait of Juan de Fuca. A possible low-relief scarp is present along the trend of the Utsalady Point fault on nearby northern Camano Island (Figs. 2 and 11) to the southeast, where offshore seismic-reflection data suggest deformation is distributed across a broad zone (Johnson *et al.*, 2001). Much of this zone is characterized by large landslides. Further investigations, including geologic mapping and possible trenching, are needed to evaluate the relation of these landforms to the fault zone.

At Teeka trench, we report cumulative slip of 2.20 to 2.65 m in one earthquake (derived from combined estimates of vertical and lateral slip), and at Duffers trench, the minimum vertical slip was 1.1 m (two-event hypothesis) or 2.1 m (one-event hypothesis). Assuming that these are maximum surface displacements (because the trenches were located where the scarps are highest), the empirical relation-

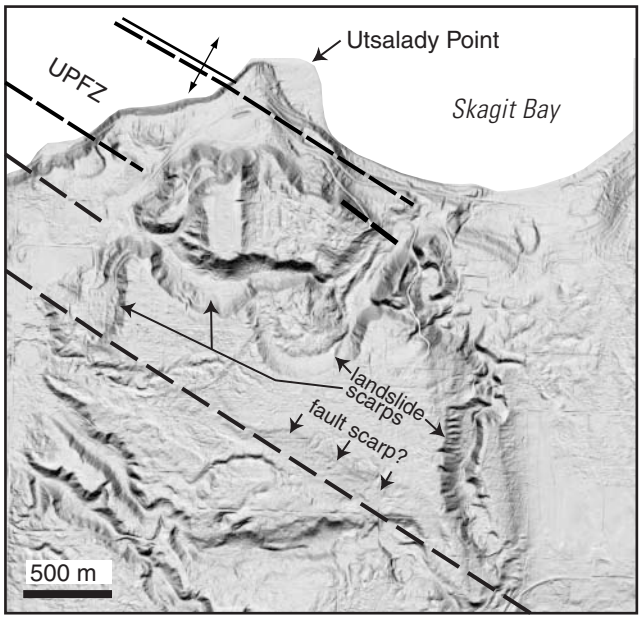

Figure 11. ALSM "bald-earth" image showing southwest projection of Utsalady Point fault zone (UPFZ) on northern Camano Island. Faults and folds based on offshore seismic-reflection data and onland exposures (Johnson *et al.*, 2001). The area is characterized by large landslides and subtle northwest-trending landforms that may have tectonic origins.

ships of Wells and Coppersmith (1994; their figure 10) suggest earthquakes in the range of *M* 6.7 to 7.0 for these events.

Few data are available that can be used to estimate a fault slip rate. Johnson *et al.* (2001) suggested a minimum Quaternary vertical slip rate of about 0.15 mm/yr on the Utsalady Point fault, based primarily on interpretations of offshore seismic-reflection profiles. They postulated left-lateral slip based on regional deformation patterns but had no data to constrain a lateral slip rate.

Our evidence for one or possibly two (favored interpretation) late Holocene earthquakes on the fault is insufficient to estimate an earthquake recurrence interval. The trench stratigraphy should record all postglacial (last ~15 ka) events on the Utsalady Point fault. Our estimates of vertical offset range between 1.0 to 1.3 m for the two-event hypothesis, and 1.15 to 2.10 cm for the one-event hypothesis. If these are typical surface displacements, then the minimum frequency of large ground-rupturing earthquakes on the Utsalady Point fault is about 6700 to 14,000 years using the minimum vertical slip rate cited previously. The recurrence interval for large earthquakes on the Utsalady Point fault thus appears to be highly irregular, with one or two events occurring in the late Holocene and no evidence for other earthquakes in the last 16 ka. Nelson *et al.* (2003) discovered a similar cluster of late Holocene earthquakes on a backthrust in the Seattle fault zone where trenching revealed evidence of three or four late Holocene earthquakes but, at most, only one other postglacial event.

Possible Regional Effects

Johnson *et al.* (2001) described outcrops of faulted latest Pleistocene (~ 21 to 15 ka) strata at two sites on Camano Island in the Utsalady Point fault zone. Although there are no prominent scarps at either site, some of the faulting at these sites may have occurred during the late Holocene earthquake(s) described in our trenches. Strong ground shaking could have also induced large landslides on northern Camano Island (Fig. 11). Strong ground motion associated with the most recent earthquake on the Utsalady Point fault may have also caused liquefaction dated to about A.D. 1430 to 1640 in the Snohomish River delta (Bourgeois and Johnson, 2001) (Fig. 1). The potential for strong ground motions generated by earthquakes on the Utsalady Point fault will add substantially to regional seismic hazard assessments (e.g., Frankel *et al*., 2002).

Because the Utsalady Point fault extends westward into the eastern Strait of Juan de Fuca and probably ruptured the seafloor during large earthquakes, it may have generated local tsunamis. Williams and Hutchinson (2000) identified four tsunami deposits in the nearby Swantown Marsh on Whidbey Island (Fig. 2), all of which occurred in the period of ~2200 to 1100 cal yr B.P., coinciding with the postulated first late Holocene earthquake on the Utsalady Point fault. They noted that only two of the Swantown tsunami beds correlate with known plate-boundary earthquakes (e.g., Atwater and Hemphill-Haley, 1997) and suggested that the other two were caused by earthquakes on local faults in the Strait of Juan de Fuca or by large submarine landslides. Similarly, Williams *et al.* (2004) described at least six and possibly nine late Holocene tsunami beds in a marsh at the head of Discovery Bay on the south shore of the Strait of Juan de Fuca (Fig. 1). The ages of four beds correlate with plate-boundary earthquakes (e.g., Atwater and Hemphill-Haley, 1997). Another tsunami bed, dated at about 500 to 300 cal yr B.P., coincides with the time of the most recent earthquake on the Utsalady Point fault. As many as five tsunami beds at Discovery Bay are in the age range of the penultimate earthquake on the Utsalady Point fault, a period in which only two plate-boundary earthquakes have been documented. Given the present lack of evidence for other crustal earthquakes in the Strait of Juan de Fuca region in the past 2500 years, it appears likely that submarine rupture on the Utsalady Point fault has produced tsunamis.

Frequency of Crustal-Fault Earthquakes in the Puget Lowland

Recent paleoseismologic studies in the Puget Lowland have documented evidence of five to seven large, ground-rupturing earthquakes on upper-plate (crustal) faults in the past 3000 years. This article describes evidence of at least one and probably two ground-rupturing, late Holocene earthquakes on an active fault in the northern Puget Lowland. Nelson *et al.* (2003) documented at least three and possibly four ground-rupturing earthquakes in the Seattle fault zone in the past 2500 years. Sherrod *et al.* (2004) presented trench evidence for at least one earthquake on the Tacoma fault (Brocher *et al.*, 2001; Johnson *et al.*, 2004) about 1100 years ago, but this deformation may be coseismic with an earthquake on the Seattle fault. Kelsey *et al*. (2004) documented one large earthquake on the northeast strand of the southern Whidbey Island fault (Fig. 2) (Johnson *et al.*, 1996) about 3000 cal yr B.P. Based on this information, the average recurrence of large earthquakes on upper-plate faults in the Puget Lowland is about 428 to 600 years. However, this rate is clearly a maximum because all of these paleoseismological studies have been conducted since 1998 when ALSM made much of this work possible. As more possible tectonic landforms are studied, additional earthquakes will be documented, resulting in increasingly short recurrence estimates.

Hyndman *et al.* (2003) estimated a recurrence interval for large upper-plate fault earthquakes in the Puget Lowland-Georgia Strait region to be about 200 years based on the seismic moment rate required to accommodate the deformation rates derived from Global Positioning System (GPS) and geologic data. They inferred that about one-half of the upper-plate events occurred shortly after great plate-boundary earthquakes. Our inferred age for the most recent earthquake on the Utsalady Point fault (A.D. 1550 to 1850) spans the

age (A.D. 1700) of the most recent plate-boundary event (Satake *et al.*, 1996; Atwater and Hemphill-Haley, 1997) and could be one of these "triggered" earthquakes. However, our ability to date the recent event on the Utsalady Point fault earthquake may never be precise enough to make this correlation conclusive. Regardless, the most recent event on the Utsalady Point fault earthquake is the youngest known, large, upper-plate fault earthquake in the Puget Lowland.

Significance for Regional Deformation Models

Regionally, GPS data document relatively large southwest–northeast shortening in western Washington that records interseismic strain accumulation subparallel to the plate convergence vector (e.g., Khazaradze *et al.*, 1999; Miller *et al.*, 2001; Mazzotti *et al.*, 2002). Most of this strain is thought to be elastic, recoverable after large plate-boundary earthquakes. After modeling the recovery of the upper plate with elastic dislocation models, "residual" motions in the Puget Lowland and south Georgia Strait predict about 5 to 7 mm/yr of north–south shortening, which is assumed to be distributed on faults and folds. Thrust and reverse faulting on east-trending structures in the Puget Lowland, such as the Seattle and Tacoma faults (Johnson *et al.*, 1994, 1999, 2004; Blakely *et al*., 2002; Nelson *et al.*, 2002, 2003; Sherrod *et al.*, 2004), are consistent with this modeling, whereas left-lateral slip on east-southeast trending structures such as the Utsalady Point fault is not predicted.

At least two explanations for the lateral slip are possible: (1) Current elastic dislocation models predict too much recovery after plate-boundary earthquakes and some of the east-northeast directed crustal strain in western Washington generated by shortening above a locked subduction zone is accommodated by inelastic crustal deformation. (2) Crust in the northern Puget Lowland is broken into several discrete, poorly defined, fault-bounded blocks. North–south shortening in the Puget Lowland produces clockwise rotation of the block south of the Utsalady Point fault, which results in left-lateral slip on the northern block margin. These hypotheses can not be tested with available data but could be evaluated with data from a denser GPS network in this complex, tectonically active region.

Conclusions

Trench investigations of a short scarp along the Utsalady Point fault document evidence of at least one and probably two late Holocene earthquakes. At the Teeka trench, truncation of narrow, steep-sided submarine channels reveals evidence of vertical (115 to 130 cm) and left-lateral (200 to 220 cm) fault displacement. In Duffers trench, vertical separation of 370 to 450 cm is accommodated by faulting (~210 cm) and folding (~160 to 240 cm), and an unknown amount of lateral slip is also likely. Radiocarbon ages on charcoal from buried soils, fault-related colluvium, and fissure fills suggest that earthquake-induced deformation occurred between 100 and 400 cal yr B.P., and probably between 1100 and 2200 cal yr B.P. For the two-earthquake hypothesis, we speculate that deformation at the Teeka trench in the penultimate event involved folding but no faulting. Regional relations suggest that the earthquake(s) were $M \geq \sim 6.7$ and that offshore rupture may have produced tsunamis. Based on this investigation and related recent studies, the maximum recurrence for large ground-rupturing crustal-fault earthquakes in the Puget Lowland is about 400 to 600 years.

Acknowledgments

Trenching on northern Whidbey Island was made possible through the permission and great hospitality of Ray and Gail Priest and Whidbey Island Naval Air Station. Collin McGinness expertly excavated the trenches. Local logistical and planning support was provided by Ben Altz-Stamm, Sherry Davis, Doug Kelly, Steve Lombardo, and Tom Nash. Our trenching was mainly supported by the U.S. Geological Survey Earthquake Hazards Program. The ALSM survey was supported by the U.S. Geological Survey, National Aeronautic and Space Administration, Island County, and the Puget Sound Lidar Consortium. We thank Jerry Harless, Ralph Haugerud, and Craig Weaver for their work on behalf of ALSM in the Puget Lowland. Anthony Crone, Michael Machette, Gary Carver, and an anonymous reviewer provided thorough and constructive reviews.

References

Atwater, B. F., and E. Hemphill-Haley (1997). Recurrence intervals for great earthquakes of the past 3,500 years at northwestern Willapa Bay, Washington, *U.S. Geol. Survey Prof. Paper 1576*, 108 pp.

Blakely, R. J., R. E. Wells, C. S. Weaver, and S. Y. Johnson (2002). Location, structure, and seismicity of the Seattle fault, Washington, *Geol. Soc. Am. Bull.* **114,** 169–177.

Bourgeois, J., and S. Y. Johnson (2001). Geologic evidence of earthquakes in the Snohomish delta, *Geol. Soc. Am. Bull.* **113,** 482–494.

Brocher, T. M., T. Parsons, R. J. Blakely, N. I. Christensen, M. A. Fisher, and R. E. Wells the SHIPS Working Group (2001). Upper crustal structure in Puget Lowland, Washington: results from the 1998 seismic hazards investigation in Puget Sound, *J. Geophys. Res.* **106,** 13,541–13,564.

Bronk Ramsey, C. (1998). Probability and dating, *Radiocarbon* **40,** 461–474.

Christie-Blick, N., and K. T. Biddle (1985). Deformation and basin formation along strike-slip faults, in *Strike-slip Deformation, Basin Formation, and Sedimentation*, K. T. Biddle and N. Christie-Blick (Editors), *Soc. Econ. Paleontol. Mineral. Spec. Pub.* **37**, 1–34.

Clowes, R. M., M. T. Brandon, A. G. Green, C. J. Yorath, A. Sutherland Brown, E. R. Kanesewich, and C. J. Spencer (1987). LITHOPROBE, southern Vancouver Island: Cenozoic subduction complex imaged by deep seismic reflections, *Can. J. Earth Sci.* **24,** 31–51.

Dethier, D. P., F. Pessl, Jr., R. F. Keuler, M. A. Balzarini, and D. R. Pevear (1995). Late Wisconsin glaciomarine deposition and isostatic rebound, northern Puget Lowland, Washington, *Geol. Soc. Am. Bull.* **107,** 1288–1303.

Domack, E. W. (1982). Facies of late Pleistocene glacial-marine sediments on Whidbey Island, Washington, *Ph.D. thesis*, Rice University, Houston, 253 pp.

Domack, E. W. (1983). Facies of late Pleistocene glacial-marine sediments on Whidbey Island, Washington: an isostatic glacial-marine sequence, in *Glacial-Marine Sedimentation*, B. F. Molnia (Editor), Plenum, New York, 535–570.

Frankel, A. D., M. D. Peterson, C. S. Mueller, K. M. Haller, R. L. Wheeler,

E. V. Leyendecker, R. L. Wesson, S. C. Harmsen, C. H. Cramer, D. M. Perkins, and K. S. Rukstales (2002). Documentation for the 2002 update of the National seismic hazard maps, *U.S. Geol. Surv. Open-File Rept. 02-420* (available at http://geohazards.cr.usgs.gov/eq/).

Gavin, D. G. (2000). Holocene fire history of a coastal temperate rain forest, Vancouver Island, British Columbia, *Ph.D. Thesis*, University of Washington, Seattle, 133 pp.

Gower, H. D., J. C. Yount, and R. S. Crosson (1985). Seismotectonic map of the Puget Sound region, Washington. *U.S. Geol. Surv. Map I-1613*, scale 1:250,000.

Harding, D. J., and G. S. Berghoff (2000). Fault scarp detection beneath dense vegetation cover: airborne lidar mapping of the Seattle fault zone, Bainbridge Island, Washington State, in *Proc. Am. Soc. Photogram. Rem. Sens. Ann. Conf*., Washington, D.C., 9 pp (available at http://duff.geology.washington.edu/data/raster/lidar/harding.pdf).

Haugerud, R. A., D. J. Harding, S. Y. Johnson, J. Harless, C. S. Weaver, and B. L. Sherrod (2003). Lidar topography for earth science studies in the Puget Lowland, Washington, *GSA Today* **13,** 4–10.

Hobbs, S. W., and W. T. Pecora (1941). Nickel-gold deposit near Mount Vernon, Skagit County, Washington, Chapter D of Strategic minerals investigations, 1941, short papers and preliminary reports, Part 1, *U.S. Geol. Surv. Bull.* **931,** 57–78.

Hyndman, R. D., S. Mazzotti, D. Wiechert, and G. C. Rogers (2003). Frequency of large crustal earthquakes in Puget Sound—south Georgia Strait predicted from geodetic and geologic deformation rates, *J. Geophys. Res*. **108,** no. **B1**, 2033, doi 10.1029/2001JB001710.

Johnson, S. Y., R. J. Blakely, W. J. Stephenson, S. V. Dadisman, and M. A. Fisher (2004). Active shortening of the Cascadia forearc and implications for seismic hazards of the Puget Lowland, *Tectonics* **23,** TC1011, doi 10.1029/2003TC001507.

Johnson, S. Y., S. V. Dadisman, J. R. Childs, and W. D. Stanley (1999). Active tectonics of the Seattle fault and central Puget Lowland: implications for earthquake hazards, *Geol. Soc. Am. Bull.* **111,** 1042–1053.

Johnson, S. Y., S. V. Dadisman, D. C. Mosher, R. J. Blakely, and J. R. Childs (2001). Active tectonics of the Devils Mountain fault and related structures, northern Puget Lowland and eastern Strait of Juan de Fuca region, Pacific Northwest, *U.S. Geol. Surv. Profess. Pap. 1643*, 46 pp., 2 plates.

Johnson, S. Y., A. R. Nelson, S. F. Personius, R. E. Wells, H. M. Kelsey, B. L. Sherrod, K. Okumura, R. Koehler, III, R. Witter, L.-A. Bradley, and D. J. Harding (2003). Maps and data from a trench investigation of the Utsalady Point fault, Whidbey Island, Washington, *U.S. Geol. Surv. Misc. Invest. Map 2420*, 1 plate.

Johnson, S. Y., C. J. Potter, and J. M. Armentrout (1994). Origin and evolution of the Seattle basin and Seattle fault, *Geology* **22,** 71–74.

Johnson, S. Y., C. J. Potter, J. M. Armentrout, J. J. Miller, C. Finn, and C. S. Weaver (1996). The southern Whidbey Island fault, an active structure in the Puget Lowland, Washington, *Geol. Soc. Am. Bull.* **108,** 334–354.

Kanamori, H. (1995). The Kobe (Hyobo-ken Nanbu), Japan, earthquake of January 16, 1995, *Seism. Res. Lett*. **66,** 6–10.

Kelsey, H. M., B. L. Sherrod, S. Y. Johnson, and S. V. Dadisman (2004). Land-level changes from a late Holocene earthquake in the northern Puget Lowland, Washington, *Geology* **32,** 469–472.

Khazaradze, G., A. Qamar, and H. Dragert (1999). Tectonic deformation in western Washington from continuous GPS measurements, *Geophys. Res. Lett.* **26,** 3153–3156.

Loveseth, T. P. (1975). The Devils Mountain fault zone, northwestern Washington, *M.S. Thesis*, University of Washington, Seattle, 29 pp.

Ludwin, R. S. (1999). Cascadia megathrust earthquakes in Pacific Northwest Indian myths and legends, *Tech. Rept., U.S. Geol. Surv. Grant 1434-HQ-97-GR-03166* (available at www.geophys.washington.edu/SEIS/PNSN/HIST_CAT/STORIES/draft1.html).

Ludwin, R. S., and A. I. Qamar (1995). Historic seismicity catalog and macroseismic accounts for Cascadia, 1793-1929, *Final Tech. Rept., 1993–1995, U.S. Geol. Surv. Grant 1434-93-G-2323*, 72 pp.

Mazzotti, S., H. Dragert, R. D. Hyndman, M. M. Miller, and J. A. Henton (2002). GPS deformation in a region of high crustal seismicity, N. Cascadia forearc, *Earth Planet. Sci. Lett.* **198,** 41–18.

McCalpin, J. P. (1996). *Paleoseismology*, Academic Press, Orlando, Florida, 608 pp.

Miller, M. M., D. J. Miller, C. M. Rubin, H. Dragert, K. Wang, A. Qamar, and C. Goldfinger (2001). GPS-determination of along-strike variation in Cascadia margin kinematics: Implications for relative plate motion, subduction zone coupling, and permanent deformation, *Tectonics* **20,** 161–176.

Mosher, D. C., and S. Y. Johnson (Editors) (2001). Neotectonics of the eastern Strait of Juan de Fuca; a digital geological and geophysical atlas, *Geol. Surv. Canada Open File Rept. D3931* (CD digital product), 18 maps, text and figures.

Nelson, A. R., S. Y. Johnson, H. M. Kelsey, R. E. Wells, B. L. Sherrod, S. K. Pezzopane, L. Bradley III, and R. D. Koehler (2003). Late Holocene earthquakes on the Toe Jam Hill fault, Seattle fault zone, Bainbridge Island, Washington, *Geol. Soc. Am. Bull.* **115,** 1388–1403.

Nelson, A. R., S. Y. Johnson, R. E. Wells, S. K. Pezzopane, H. M. Kelsey, B. L. Sherrod, L.-A. Bradley III, R. D. Koehler, R. C. Bucknam, R. A. Haugerud, and W. T. LaPrade (2002). Field and laboratory data from an earthquake history study of the Toe Jam Hill fault, Bainbridge Island, Washington, *U.S. Geol. Surv. Open-File Rept. 02-60*, 37 pp., 2 plates.

Pollitz, F. P., and I. S. Sacks (1997). The 1995 Kobe, Japan, earthquake: a long delayed aftershock of the offshore 1944 Tonankai and 1946 Nankaido earthquakes, *Bull. Seism. Soc. Am.* **87,** 1–10.

Porter, S. C., and T. W. Swanson (1998). Radiocarbon age constraints on advance and retreat of the Puget Lobe of the Cordilleran ice sheet during the last glaciation, *Quat. Res.* **50,** 205–213.

Satake, K., K. Shimazaki, Y. Tsuji, and K. Ueda (1996), Time and size of a giant earthquake in Cascadia inferred from Japanese tsunami record of January 1700, *Nature* **379,** 246–249.

Sherrod, B. L., T. M. Brocher, C. S. Weaver, R. C. Bucknam, R. J. Blakely, H. M. Kelsey, A. R. Nelson, and R. A. Haugerud (2004). Holocene fault scarps near Tacoma, Washington, *Geology* **32,** 9–12.

Stuiver, M., P. J. Reimer, E. Bard, J. W. Beck, G. S. Burr, K. A. Hughen, B. Kromer, G. McCormac, J. v. D. Plicht, and M. Spurk (1998). INTCAL98 radiocarbon age calibration, 24,000-0 cal BP, *Radiocarbon* **40,** 1041–1084.

Tabor, R. W. (1994). Late Mesozoic and possible early Tertiary accretion in western Washington state: the Helena-Haystack melange and the Darrington-Devils Mountain fault zone, *Geol. Soc. Am. Bull.* **106,** 217–232.

Taylor, R. E., M. Stuiver, and P. J. Reimer (1996). Development and extension of the calibration of the radiocarbon time scale: archeological applications, *Quat. Sci. Rev*. **15,** 655–668.

Wells, D. L., and K. J. Coppersmith (1994). New empirical relationships among magnitude, rupture length, rupture area, and surface displacement, *Bull. Seism. Soc. Am.* **84,** 974–1002.

Wells, R. E., C. S. Weaver, and R. J. Blakely (1998). Fore-arc migration in Cascadia and its neotectonic significance, *Geology* **26,** 759–762.

Williams, H., and I. Hutchinson (2000). Stratigraphic and microfossil evidence for late Holocene tsunamis at Swantown marsh, Whidbey Island, Washington, *Quat. Res.* **54,** 218–227.

Williams, H., I. Hutchinson, and A. Nelson (2004). Multiple sources for late Holocene tsunamis at Discovery Bay, Washington State, USA, *The Holocene* (in press).

U.S. Geological Survey
400 Natural Bridges Drive
Santa Cruz, California 95060
(S.Y.J.)

U.S. Geological Survey
Mail Stop 966, Box 25046
Denver, Colorado 80225
(A.R.N., S.F.P., L.-A.B.)

U.S. Geological Survey
Mail Stop 975, 345 Middlefield Rd.
Menlo Park, California 94025
(R.E.W.)

Department of Geology
Humboldt State University
Arcata, California 95521
(H.M.K.)

U.S. Geological Survey
Department of Earth and Space Science
University of Washington
Seattle, Washington 98195
(B.L.S.)

Department of Geography
Hiroshima University
1-2-3 Hagamiyama
Higashi-Horoshima, 739-8522 Japan
(K.O.)

William Lettis and Assoc., Inc.
1777 Botelho Drive, Suite 262
Walnut Creek, California 94596
(R.K., R.C.W.)

NASA
Goddard Space Flight Center, MC 921
Greenbelt, Maryland 20771
(D.J.H.)

Manuscript received 12 March 2004.